MRI Compatible Robotic Dosimeter System for Safety Assessment of Medical Implants

Daniel E. Martinez, Heriberto A. Nieves-Vazquez, Yusuf S. Yaras, Alexey Khotimsky, Ben Skowronski, Lee Bradley, John Oshinski, F. Levent Degertekin, *Fellow, IEEE*, Jun Ueda, *Senior Member, IEEE*

***Abstract*— Magnetic Resonance Imaging (MRI) is considered a safe imaging modality since there is no use of ionizing radiation. However, safety concerns still arise due to Radiofrequency (RF)-induced heating of electrically conducting structures such as medical implants. While recent advancements in robotics and sensors have enabled the measurement of temperature and electric fields outside the MRI setting, the heat generated by electromagnetic components within an MRI scanner still poses a challenge. This paper proposes the use of an MRI-compatible robot to accurately move and position a novel MRI-compatible sensor at different points in a gel phantom to generate heat and electric field maps around implantable medical devices. The effectiveness of the system is demonstrated by measuring a heat map around an abandoned pacemaker lead. The system provides a novel method of medical device safety evaluation in a clinical MRI setting.**

***Index Terms*— MRI safety, RF-induced heating, implantable devices, MRI compatible robot, Piezoelectric actuation**

I. Introduction

Magnetic resonance imaging (MRI) is a medical imaging technique that uses strong magnetic fields and radio frequency (RF) waves to generate detailed images of the internal structures of the body. MRI is considered to be a safe imaging modality, as it doesn't use ionizing radiation such as X-rays or CT scans. However, there are important safety considerations due to the use of strong magnetic and high-amplitude RF fields [1]. The primary heating mechanism is the joule heating of the electrically conductive tissue due to Eddy current formation by the fast-changing RF field, especially the tangential electric (E) field component [2]. The RF-induced heating is further exacerbated by the presence of electrically conducting structures such as pacemaker leads, neurostimulators, or metallic implants in the body. Depending on the geometry, device orientation, material composition, and termination impedance, conducting structures can act as resonant antennae, which lead to localized high RF power deposition in the vicinity of these structures. ASTM F2182-19a and ISO/TS 10974:2018 standards are used for the MRI safety assessment of medical implants [3] [4]. In order to mitigate the risk of RF induced heating, the absorbed RF energy or specific absorption rate (SAR) should be limited to keep the temperature below 39C (2C temperature increase) [5]. The primary focus of ASTM F2182 is to determine the level of RF-induced heating by measuring temperature rise near implants. Since temperature measurements are required during the MRI scan for this standard, MRI-compatible fiber optic temperature sensors are used to minimize the heating induced by the sensors themselves. Technical specification of ISO/TS 10974:2018 requires measurement of tangential E field around active implantable medical devices (AIMDs). It is important to note that both temperature and E field can be used to measure SAR. Measurements for both standards are only taken at the predicted hot spots due to the lack of MRI compatible precision positioning system. However, temperature and E field maps are required to identify the potential hot spot locations and RF-heating distribution around the implants. Standalone birdcage coils have been used to simulate the RF field inside the MRI scanner so that regular (not MRI-compatible) robotic positioning systems can be used for mapping purposes [6]. However, these studies are limited to bench-top experiments and do not allow in-situ measurements.

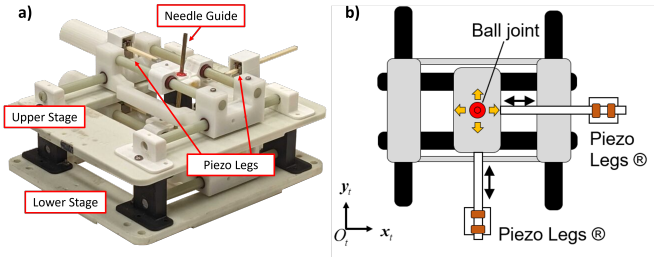

Fig. 1. The AutoSPINe Robot. a) Photo of the direct-drive parallel plane mechanism, b) X-Y linear stage driven by linear piezoelectric actuators. The bottom x-y stage is functionally identical to the upper stage.

In this paper, we propose a dosimeter system for measuring RF energy absorption that integrates a previously developed MRI-compatible robotic positioning system that can navigate an endpoint with greater accuracy than MRI resolution [7] and a novel acousto-optic(AO) sensor capable of measuring both temperature and electrical field in an MRI setting [8] to create a procedure for generating heat maps for evaluating the safety of passive or active implantable devices in MRI. An RF-induced heating experiment of an implantable medical device inside a gel phantom replicating thermal and electrical conductivity of human tissue is performed to verify the effectiveness of the proposed system.

D.E. Martinez, H. Nieves-Vazquez, Y. Yaras, A. Khotimsky, B. Skowronski, L. Bradley, F L. Degertekin, and J. Ueda are with the Woodruff School of Mechanical Engineering, Georgia Institute of Technology, Atlanta, GA. J. Oshinski is with Georgia Institute of Technology, Wallace H. Coulter Department of Biomedical Engineering, and Emory University, Department of Radiology and Imaging Sciences, Atlanta, GA, USA

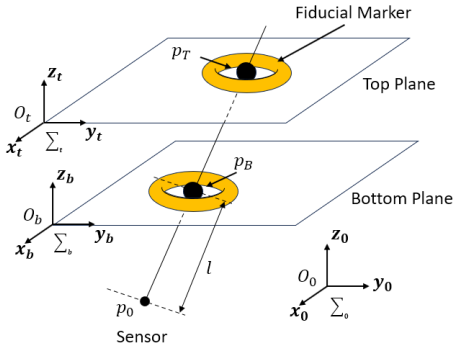

Fig. 2. AutoSPINe kinematics.

II. Methods

A. Robotic System

In this paper, the AutoSPINe, a direct-drive parallel plane mechanism (D^2P^2) previously developed for therapeutic spinal injections in [9] was adapted as shown in Figure 1(a). Each plane is a planar x-y positioning mechanism, positioning a ball joint at the center of the stage, driven by orthogonally located linear piezoelectric actuators (PIEZO LEGS, Micromo, Clearwater FL, USA) as shown in Figure 1(b). The upper and lower ball joints can move independently, controlling 4 Degrees of Freedom (DOF) of the needle guide. A mounting rod was designed to attach the AO sensor described later in the paper below the robot at the end of a rod inserted through the needle guide. The fifth and sixth DOFs, i.e, insertion depth (along the direction of the needle guide) and rod rotation, are controlled manually by the user through adjustments in the mounting rod. Because the actual distance between the ball joints is dependent on the orientation, the cannula is fixed in the lower joint, while the upper joint allows the cannula to slide through the center of the ball joint. MRI viability of this robot was verified and reported in [9].

Forward kinematics is presented to represent the needle guide position in the absolute coordinate frame using ball joint positions in the planar coordinate frames fixed to individual x-y stages. Let ${}^t\boldsymbol{p}_{BT} = \begin{bmatrix} x_t \\ y_t \end{bmatrix}$ be the ball position of the top x-y stage with respect to the coordinate frame fixed to it as shown in Figure 2. Similarity, let ${}^b\boldsymbol{p}_{BB} = \begin{bmatrix} x_b \\ y_b \end{bmatrix}$ be the ball position of the bottom x-y stage. Defining ${}^t\boldsymbol{P}_{BT} = \begin{bmatrix} {}^t\boldsymbol{p}_{BT} \\ 1 \end{bmatrix}$ and ${}^b\boldsymbol{P}_{BB} = \begin{bmatrix} {}^b\boldsymbol{p}_{BB} \\ 1 \end{bmatrix}$, homogeneous transformation, ${}^0\boldsymbol{P}_{BT} = {}^0\boldsymbol{T}_t\,{}^t\boldsymbol{P}_{BT}$ and ${}^0\boldsymbol{P}_{BB} = {}^0\boldsymbol{T}_t\,{}^t\boldsymbol{P}_{BB}$ provides the ball positions with respect to the base coordinate frame $\sum_0$ where ${}^0\boldsymbol{T}_t$ and ${}^0\boldsymbol{T}_b$ are homogeneous transformation matrices.

B. Control of robot and sensor position in MRI

Imaging of two fiducial markers built into the robot part that houses the ball joints enables detection of the 4-DOF position and orientation. The ball joint housing is manufactured with a hollow torus concentric to the ball joint that is filled with vitamin E for visibility in MRI. The toroidal exterior of the fiducial markers makes their outer diameter appear as circles in the coronal MRI slices. Running a circle detection algorithm on an image slice with the fiducial marker visible returns the location of the fiducial marker in the image. The 4-DOF position and orientation can then be calculated from the location of the two markers. This process is outlined in Figure 3. The forward kinematics outlined in section II-A is then used to calculate the sensor position, with the insertion depth set by the manually controlled sensor mounting rod.

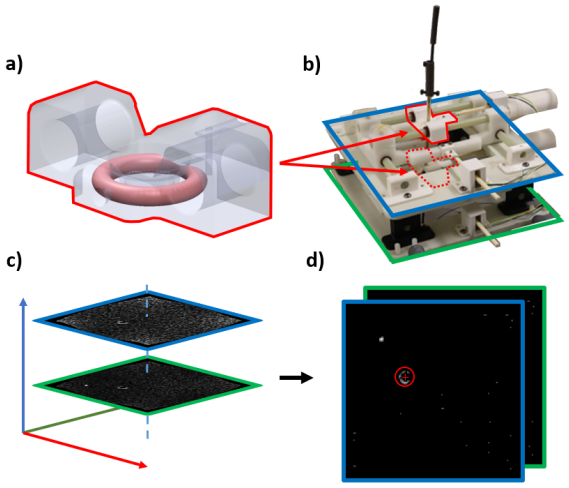

Fig. 3. Visualization of fiducial markers in MRI scan. a) shows the 3D model of the robot part containing the toroidal fiducial, b) shows the physical robot highlighting the two planes and fiducial containing part, c) represents the MRI scan highlighting the coronal robot plane slices, d) shows the location of the fiducials in the slices.

Image Jacobians relate small actuator displacements, $\Delta x_t, \Delta y_t, \Delta x_b, \Delta y_b$, and resultant ball joint displacements expressed in the global coordinate frame, $\Delta^0\boldsymbol{P}_{BT}$ and $\Delta^0\boldsymbol{P}_{BB}$. Matching ${}^0\boldsymbol{P}_{BT}$ and ${}^0\boldsymbol{P}_{BB}$ with the ones of the desired sensor position, ${}^0\boldsymbol{P}_{BTd}$ and ${}^0\boldsymbol{P}_{BBd}$, solves the inverse kinematics. Note that the two X-Y stages can be operated independently of each other. The solution is unique as long as ${}^0\boldsymbol{P}_{BT}$ and ${}^0\boldsymbol{P}_{BB}$ exist, i.e., unless the needle is not completely orthogonal to the parallel planes. Use of image Jacobians allow for the control of kinematics to solely be done in the global frame defined by the imaging modality. The image-guided positioning is performed in an iterative fashion until the distance to the desired target point (what we refer to as positioning error) is below a desired threshold.

C. Acousto-optic Sensor Design

The acousto-optic (AO) sensor consists of a piezoelectric transducer mechanically coupled to a Fiber Bragg Grating (FBG) at the distal end of the optical fiber. Electric field sensing relies on the inherent E field sensitivity of piezoelectric transducers [10] whereas temperature sensing relies on the inherent sensitivity of FBGs to ambient temperature change [11]. A schematic overview of the measurement set-up and a close-up image of the AO sensor are shown in

Figure 4. Optical read out is achieved through a side slope detection method [12]. A low noise InGaAs photodetector and a narrow linewidth laser are used for probing the FBG at a wavelength on a slope in the reflection spectrum. The central notch was used for E field detection, as it provides the highest sensitivity, whereas one of the side lobes was used for temperature measurement for the increased range as shown in Figure 5. AC coupled photodetector output is monitored for the time-domain (high frequency, low amplitude) E field measurement, whereas the DC coupled photodetector output is monitored for slow changing temperature measurements. In this particular sensor, a π-phase shifted FBG sensor was used with a 0.4 pm bandwidth and a central wavelength of 1550 nm (Teraxion Inc., Quebec, Canada) embedded in a 125 μm diameter optical fiber. A 140 μm thick 36Y-cut LiNbO3 piezoelectric crystal was used for E field detection. Note that this particular piezoelectric transducer works at Larmor frequencies of 0.55T (23.6 MHz) and 1.5T (64 MHz) MRI systems.

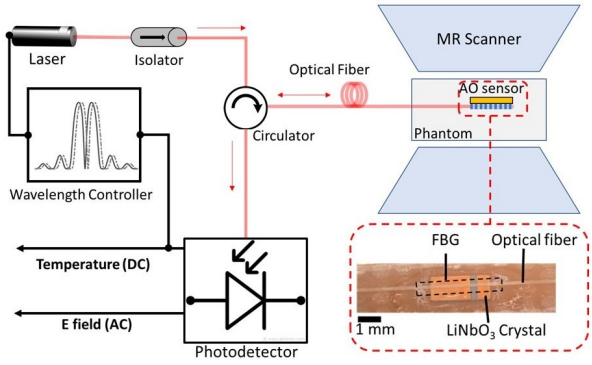

Fig. 4. Schematic overview and close up photo of the AO sensor.

D. Gel Phantom Preparation

RF-induced heating of an implantable medical device was simulated using a gel phantom which mimics electromagnetic properties of the human tissue; conductivity of 0.47 S/m and dielectric constant of 81. 26.4 L of gelled saline solution was prepared with 1.32 g/L NaCl and 10 g/L polyacrylic acid (PAA) in water as specified in ASTM F2182 [3]. Electrical properties of the phantom were measured with a multiparameter electrochemistry meter (Oakton Model CON 6+, USA) and the conductivity of the phantom was adjusted according to the specification before each experiment to ensure consistency between different experiments. The phantom was contained in an acrylic box and mounted under the robot system as shown in Figure 7.

E. Specific MRI Sequences

The imaging sequence used for the visualization of the fiducial markers was performed with a turbo spin echo sequence (flip angle, 90°; TR, 910 ms; TE, 104ms; slice thickness, 3 mm; bandwidth, 16 kHz; and matrix size, 128 $\times$ 128)

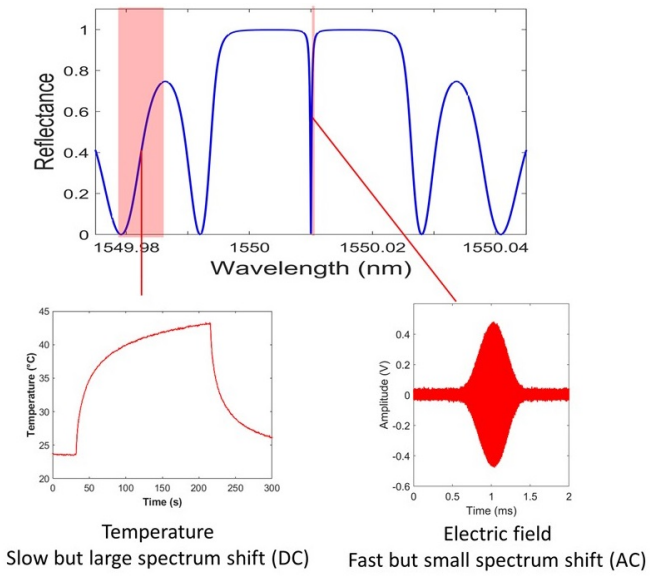

Fig. 5. Reflection spectrum of a π-phase shifted FBG showing different laser wavelengths for temperature and E field probing. The side slope of the central notch (the highest sensitivity) was used for E field measurement whereas one of the side lobes (large dynamic range) was used for temperature measurement.

The heating sequence used for the temperature measurements was performed using a turbo spin echo (TSE) sequence (flip angle, 90°; TR, 425 ms; TE, 8.4 ms; slice thickness, 10 mm; bandwidth, 16 kHz; and matrix size, 256 $\times$ 256).

F. Example Implantable Medical Device: Pacemaker Lead

Abandoned leads are leads that are disconnected from the implantable cardioverter defibrillator (ICD), usually abandoned due to malfunction or device upgrade. As these are legacy devices, most of them were not tested for MRI safety by the manufacturers, rendering the prediction of the RF-induced heating profile quite challenging [13]. Thus, an abandoned lead was selected as the test implant to demonstrate the functionality of the system. A conventional ICD lead with three lead connector plugs (Boston Scientific Reliance, USA) was retrieved from a patient by an electrophysiologist. The abandoned lead was placed inside the phantom and oriented as it would be in the patient. The proximal end of the lead was left un-terminated. The experimental set-up is shown in Figure 7.

G. Heat Map Generation

Characterization of the RF-induced heating is stored as a 3D heat map for ease of visualization and understanding of the heating relative to the location of the implantable device. The heat map is defined as a point cloud with temperature values stored at each point. It is worth noting that the point cloud is not limited to a Cartesian grid. The robot's positioning capabilities allow for the collection of data at any point desired, and therefore the point cloud can be defined as any set of points that would be of interest to analyze the spatial heating. The desired set of points is converted

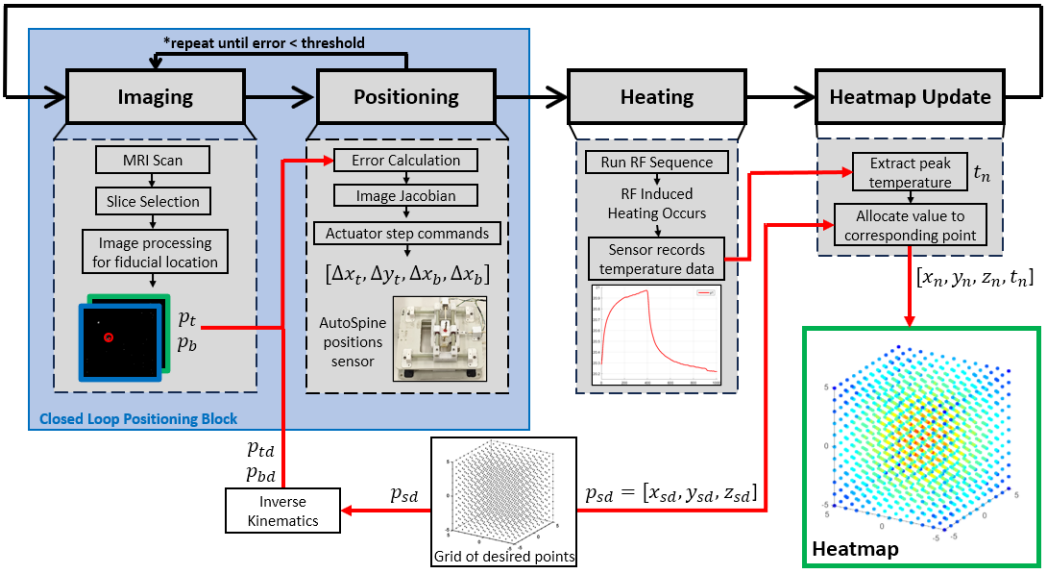

Fig. 6. Process flowchart outlining the procedure for populating a heatmap with the measured RF-induced heating.

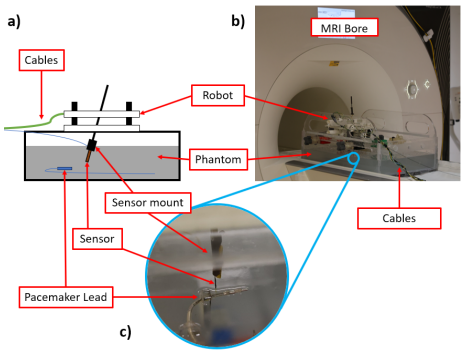

Fig. 7. a) Illustrates the experimental set-up, b) shows the system and phantom on the MRI bed, c) shows a close-up of the sensor and pacemaker lead in the phantom.

to corresponding robot ball joint positions by using the inverse kinematics solutions. The heat map is then generated iteratively by populating the point cloud with temperature values measured at each point during the heating sequence as outlined in Figure 6.

III. Results

The system was tested with a 3T MRI scanner (Magnetom Prisma, Siemens Healthineers, Germany). Since the E field sensing capability of the acousto-optic sensor is currently compatible with 0.55T and 1.5T MRI systems, only temperature measurements were collected as preliminary data presented here. At the beginning of the experiments, the temperature output of the AO sensor was calibrated with a commercial fiber optic temperature sensor (Osensa Innovations PRB 420 02M STM MRI, Canada). The procedure outlined in Figure 6 was followed to create a small heat map of six points along the axis of the pacemaker lead electrode. The ambient temperature during the experiments was approximately 20.2°C, which served as a baseline to finish AO sensor recordings. The initial point was approximately 1.5 mm from the tip of the atrial lead and all following points were approximately 1.1 mm apart. The heating and cooling profile for each point as well as an illustration of the position of the points is shown in Figure 8.

The highest temperature recorded as a result of the RF-induced heating was 21°C at a distance of 1.5 mm away from the pacemaker lead. The rise time to peak temperatures increased as distance to the pacemaker lead decreased. Peak temperatures and the distance from the pacemaker lead that the measurement was taken from are shown in Table I.

IV. Discussion

The highest temperature recorded in the presented study was less than 1 degree higher than the ambient temperature. Furthermore, the observed heating decreased as the sensor was positioned farther from the electrode, with heating of no more than 0.1 degree at 4.8 mm away from the electrode. The measured heating for this particular lead in this orientation was below 2 degrees, which demonstrates that abandoned and untested pacemaker leads may still be safe for use in the MRI setting [14] [15]. Detailed RF-induced heating maps around the abandoned or untested leads will increase the accessibility of MRI as a diagnostic option for patients who have been denied access to MRI due to the safety concerns . Similarly, the proposed system can quantify RF-induced heating of other implantable active or passive medical devices for MRI safety assessment.

Importantly, the recorded temperature profiles are dependent on the orientation, material types, and geometry of the implant. The proposed system is capable of measuring the heating that results from the complex interaction of these

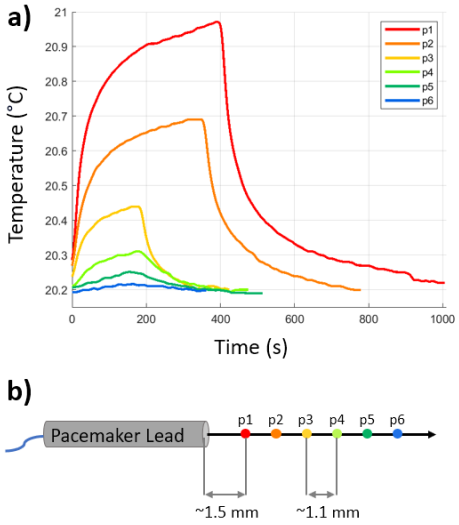

Fig. 8. a) The temperature profile measured at the points shown in b)

parameters and the MRI scanner, rather than predicting hot spot locations around the implant. The system demonstrates an alternative method for verifying the safety of medical implants during MRI scanning.

In this study, a small set of points (6 points) was selected due to limited MRI scanner time availability. Heating data collection took on average about 10 minutes at each point to cycle through the heating and cooling. This would make it very time consuming to populate a larger heat map. Future work will focus on increasing the operational frequency of AO sensor to enable E field measurements at 3T MRI. E-field measurement is much faster (few seconds) compared to temperature measurement, allowing for a much larger set of points to be evaluated within a practical time frame.

Lastly, the robot positioning was operated in an open-loop manner due to the desired number of points and desired accuracy being within the robot's open-loop capabilities. In future work with larger number of points and desired fidelity, the closed-loop positioning system will be used as demonstrated in the previous paper [7].

TABLE I

PEAK TEMPERATURES

Point:	p1	p2	p3	p4	p5	p6
Distance from Pacemaker (mm):	1.5	2.6	3.7	4.8	5.9	7
Peak Temperature (°C)	20.98	20.70	20.45	20.32	20.26	20.22

V. CONCLUSION

In this study, functionality of the proposed system for the RF induced heating measurement is demonstrated on an abandoned pacemaker lead in phantom studies under MRI. A previously developed MRI-compatible positioning robot and acousto-optic sensor were integrated successfully to develop a system for heating and E field characterization in MRI. Preliminary data in MRI was collected to generate a small heat map. The system provides a novel method for validating the safety of medical devices in MRI.

ACKNOWLEDGMENT

The first and second authors were supported by the National Science Foundation under grant number 1662029. Research on AO sensor reported in this publication was supported by the National Institutes of Health under grant number R01EB029331. The content is solely the responsibility of the authors and does not necessarily represent the official views of the National Institutes of Health.

REFERENCES

[1] J. G. Delfino, D. M. Krainak, S. A. Flesher, and D. L. Miller, "Mri-related fda adverse event reports: A 10-yr review," *Medical Physics*, vol. 46, no. 12, pp. 5562–5571, 2019.

[2] M. F. Dempsey, B. Condon, and D. M. Hadley, "Mri safety review," in *Seminars in Ultrasound, CT and MRI*, vol. 23, no. 5. Elsevier, 2002, pp. 392–401.

[3] "Standard test method for measurement of radio frequency induced heating on or near passive implants during magnetic resonance imaging," ASTM International, West Conshohocken, PA, Standard, October 2019. [Online]. Available: https://www.astm.org/f2182-19e02.html

[4] "Assessment of the safety of magnetic resonance imaging for patients with an active implantable medical device," International Organization for Standardization, Geneva, CH, Standard, April 2018. [Online]. Available: https://www.iso.org/standard/65055.html

[5] "Medical electrical equipment - part 2-33: Particular requirements for the basic safety and essential performance of magnetic resonance equipment for medical diagnosis," International Electrotechnical Commission, Standard, August 2022. [Online]. Available: https://webstore.iec.ch/publication/67211

[6] E. Neufeld, S. Kühn, G. Szekely, and N. Kuster, "Measurement, simulation and uncertainty assessment of implant heating during mri," *Physics in Medicine & Biology*, vol. 54, no. 13, p. 4151, 2009.

[7] D. E. Martinez, W. Meinhold, J. Oshinski, A.-P. Hu, and J. Ueda, "Super resolution for improved positioning of an mri-guided spinal cellular injection robot," *Journal of Medical Robotics Research*, vol. 6, no. 01n02, 2021.

[8] Y. S. Yaras, L. W. Bradley, D. K. Yildirim, O. Kocaturk, J. Oshinski, and F. L. Degertekin, "Dual mode acousto-optic rf safety sensor for electric field and temperature measurement at 1.5 t mri."

[9] W. Meinhold, D. E. Martinez, J. Oshinski, A.-P. Hu, and J. Ueda, "A direct drive parallel plane piezoelectric needle positioning robot for mri guided intraspinal injection," *IEEE Transactions on Biomedical Engineering*, vol. 68, no. 3, pp. 807–814, 2020.

[10] Y. S. Yaras, O. Kocaturk, and F. L. Degertekin, "Fbg based electric field sensor for mri safety," in *Optical Sensors*. Optica Publishing Group, 2020, pp. STu4D–7.

[11] Y. Seo and Z. J. Wang, "Measurement and evaluation of specific absorption rate and temperature elevation caused by an artificial hip joint during mri scanning," *Scientific reports*, vol. 11, no. 1, p. 1134, 2021.

[12] Y. S. Yaras, D. K. Yildirim, O. Kocaturk, and F. L. Degertekin, "Sensitivity and phase response of fbg based acousto-optic sensors for real-time mri applications," *OSA continuum*, vol. 3, no. 3, pp. 447–458, 2020.

[13] D. A. Langman, I. B. Goldberg, J. P. Finn, and D. B. Ennis, "Pacemaker lead tip heating in abandoned and pacemaker-attached leads at 1.5 tesla mri," *Journal of Magnetic Resonance Imaging*, vol. 33, no. 2, pp. 426–431, 2011.

[14] R. D. Schaller, T. Brunker, M. P. Riley, F. E. Marchlinski, S. Nazarian, and H. Litt, "Magnetic resonance imaging in patients with cardiac implantable electronic devices with abandoned leads," *JAMA cardiology*, vol. 6, no. 5, pp. 549–556, 2021.

[15] "Testing and labeling medical devices for safety in the magnetic resonance (mr) environment," Food and Drug Administration, Rockville, MD, Guidance Document, May 2021. [Online]. Available: https://www.fda.gov/regulatory-information/search-fda-guidance-documents/testing-and-labeling-medical-devices-safety-magnetic-resonance-mr-environment